Heat transfer enhancement in cryogenic quenching process

J. N. Chung[1*], S. R. Darr[1], Jun Dong[1], Hao Wang[1], J.W. Hartwig[2]

1. Cryogenics Heat Transfer Laboratory

Department of Mechanical and Aerospace Engineering

University of Florida, Gainesville, FL, 32611-6300, U.S.A.

2. *NASA Glenn Research Center, Cleveland, OH, 44135, USA*

*Corresponding author. Tel.: 352-392-9607; fax: 352-392-1071

E-mail address: jnchung@ufl.edu (J. N. Chung).

Abstract: This paper reports a heat transfer advancement in the cryogenic quenching process. An experiment was performed to evaluate the enhancement of quenching heat transfer by the use of metal tubes with low thermal conductivity coating layers. Four coating thicknesses with various coolant mass flow rates of liquid nitrogen were investigated. The results indicated that the tube inner surface coating greatly enhanced the quenching efficiency. The quenching efficiency was found to increase with increasing number of coating layers, and the efficiency also increased with decreasing mass flow rates. In general, the efficiencies cover a range between 40.6% and 80%. Comparing to the bare surface case, the percentage increase in the quenching efficiency was the minimum at 4.2% for a single coated layer at the highest flow rate and the maximum of 109.1% for four coated layers at the lowest flow rate. The coated tubes could save up to 53% in the amount of cryogen consumption.

Keywords : cryogenic fluid, quenching heat transfer, surface coating, two-phase flow, film boiling

1. Introduction

1.1. Importance of quenching heat transfer

In many convective liquid-vapor phase change heat transfer process applications, cryogenic fluids are widely used in industrial chemical processes, spacecraft and cryosurgery systems, and so on. For example, cryogens are usually used as liquid fuels such as liquid hydrogen and oxygen in the rocket industry, liquid nitrogen (LN_2) and helium are frequently used to cool superconducting magnetic device for medical applications. In these systems, proper transport, handling, and storage of cryogenic fluids are of great importance. When a cryogenic system is first started up, its walls and hardware must go through a transient chilldown period prior to reaching a steady operation. Therefore, chilldown (quenching) is the process of keeping the system adjusted to the low temperature scale which is usually several hundred degrees below the room temperature. The chilldown or quenching process is complicated, involving unsteady two-phase heat and mass transfer, and has not been fully understood.

A new breakthrough technology advancement in the quenching phase-change heat transfer processes by a low-thermal conductivity surface coating can lead to much higher quenching efficiencies, substantial energy and liquid cryogen consumption savings, and global reduction in greenhouse gas emissions. Especially for space propulsion systems, higher quenching efficiencies translate to more fuels available for making longer and deeper space missions a reality. This paper reports a breakthrough advancement on both fronts of quenching heat transfer rates and quenching efficiency.

1.2. Characteristics of quenching heat transfer

The liquid-vapor phase change heat transfer process is characterized by a “curve” that shows the functional relationship between the heat transfer surface heat flux and the surface temperature[1].

Figure 1 is a typical such curve where the heater surface heat flux, q'', is plotted against the heater surface degree of superheating, $T_W - T_{sat}$, where T_W is the surface temperature and T_{sat} is the saturation temperature corresponding to the flow system pressure. In boiling, the heating is externally supplied to the heater surface and thus, heat input can be controlled independently, such as the constant wall heat flux condition. In this case, boiling is a heat flux (independent variable) controlled process. For the heat flux controlled condition, as the heating rate is progressively increased, the process follows the route of A→B→D. In order to avoid a huge temperature jump from B→D, boiling applications usually run safely below point B for nuclear power plants.

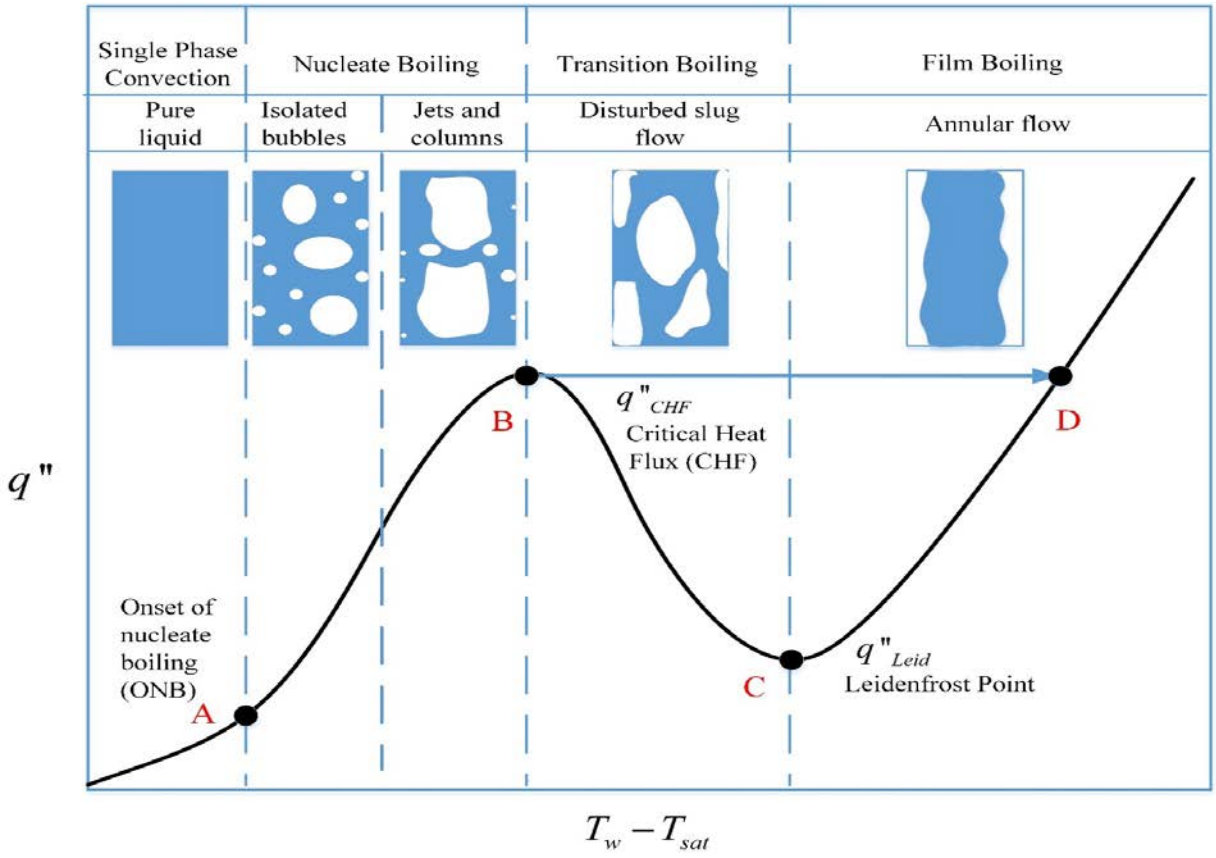

Figure 1. A typical boiling curve.

In contrast, during quenching the heat transfer wall does not have an external source of heat supply, therefore, the heat transferring out of the wall can only be supplied internally from the

thermal capacity (stored energy) of the wall. The only way to remove heat from the wall is by lowering the inner wall surface temperature using a cooling flow. Accordingly, the wall surface temperature is the independent variable and also the control parameter in quenching. In summary, quenching, a wall temperature-controlled process, is a conjugate process where the rate of heat transfer is controlled by the surface temperature variation. The rate of heat transfer to the fluid can only be associated with the temperature change of the wall inner surface. As a result, the wall surface temperature is the controlling parameter that forces the quenching process to follow the route D→C→B→A.

In boiling applications, such as that in the cooling of a nuclear reactor, taking advantage of a super high flux of heat transfer in the nucleate boiling regime with a relatively low wall surface temperature is a standard practice. The only precaution is not to exceed the critical heat flux (CHF) as any boiling process that goes beyond the CHF would enter the film boiling directly that results in a large wall temperature jump and the burnout (melting) of the heater wall (nuclear reactor fuel rod). In the past decade, many research efforts have focused on raising the CHF limit for safer and higher heat flux boiling applications. However, film boiling is the first mode of heat transfer encountered in most quenching processes, and it usually dominates the chilldown time and cannot be avoided. Due to its low heat fluxes at high wall temperatures, the quenching efficiency, in general, is extremely low. According to Shaeffer et al.[2], the average quenching efficiency that is defined as the ratio of the amount of thermal energy removed from the wall versus the maximum cooling capability of the cryogen spent in a phase change process is about 8%, highlighting the tremendous need to improve the quenching efficiency for many applications that require a cryogen as the working fluid. The key concept to increase the efficiency is to shorten the film boiling by raising the Leidenfrost point (LFP) temperature (point C in Figure 1).

1.3. Convective quenching heat transfer in tubes and pipes

Compared to the heated wall convective boiling case, the amount of literature on convective quenching heat transfer is far less. For convective quenching in tubes and pipes, most studies used water and normal room temperature fluids[3-5]. Yuan and Chung[6] and Yuan et al.[7] reported the pioneering work on liquid nitrogen (LN_2) cryogenic chilldown in conventional stainless tubes under low flow rates in both terrestrial and simulated drop-tower microgravity conditions. Both papers[6,7] established the fundamental physical understanding and benchmark data for future convective cryogenic chilldown heat transfer research. As follow-ups, LN_2 chilldown experiments of a short stainless steel tube have been carried out at low mass flux both at constant mass flux[8] and in a pulsed on/off flow[2]. Only recently has there been a thorough experimental investigation of the entire chilldown process in 1-g that reports the measured heat transfer coefficients for all boiling regimes over a large range of mass flow and thermodynamic conditions.[9,10] Another recent work[11] by the same group provided a wide ranging dataset of reduced gravity cryogenic pipe chilldown data from a parabolic flight experiment using LN_2 onboard a C9 aircraft. Heat transfer data were obtained from flowing LN_2 through a short, stainless steel (SS) pipe for developing heat transfer correlations. This experiment was an extension of 1-g experiments reported in Darr et al.[9,10]

1.4. Effects of surface modifications on boiling and quenching heat transfer

Research efforts on enhancing the heat transfer rates during quenching and chilldown processes, especially on the shortening of the inefficient film boiling regime, have been reported in recent years. The majority of those investigations were focused on making nanoscale surface texturing or depositing nanoscale particles on the heat transfer surfaces.

The so called “nanofluids”, that are pure working fluids mixed with a small amount of nanoscale particles, have been adopted by researchers to enhance single phase convective heat

transfer and convective phase-change heat transfer. The forming of a porous layer composed of nanoparticles on the heated surface is achieved by the deposition and accumulation of nano particles during convective boiling using nanofluids. The nanoparticles that were found effective are low-thermal conductivity ceramic materials such as alumina, zirconia, and silica nanoparticles. These porous layers have been reported to significantly improve the surface wettability[12,13], as shown by a reduction of the static contact angle. The contact angle reduction was thought to be due to changes in surface energy and surface morphology facilitated by the porous layers formed by nanoparticles. The high surface wettability clearly supports the boiling CHF enhancement in nanofluids[14,15]. Comprehensive reviews on the literature of boiling with nanofluids before 2007 and those before 2016 were provided by Wang and Majumdar[16] and Fang et al.[15], respectively. However, only very few reports were found that addressed the quenching heat transfer improvements by nanofluids. Quenching experiments using nanofluids have been performed on small metal spheres[17,18] and on platinum wires[19]. All three papers reported that once the low thermal conductivity nanoparticles were deposited on the surface and they would coat the surface with a nanoporous layer, the CHF and minimum heat flux were observed to increase due to the coated layer. Also the Leidenfrost temperature was raised higher, shortening the film boiling regime time. They suggested that the surface roughness increase and wettability enhancement due to nanoparticle deposition may be responsible for the premature disruption of film boiling and the acceleration of quenching.

The majority, if not all, of the hundreds of boiling heat transfer enhancement investigations by modified nanoscale surface textures were focused on the topic of nucleate boiling regime and the CHF where the heat transfer surface is heated. Two typical recent papers are reviewed here. Chen et al.[20] reported that using heater surface coated with Si and Cu nanowires could increase both the CHF and heat transfer coefficient by more than 100%. They attributed the enhancement due to the surface

becoming superhydrophilic and an increase in nucleation site density and roughness by the nano wires. Dhillon et al.[21] used nano –textured micropillar surfaces to raise the CHF. Based on a model they predicted CHF maxima and found out that there are optimal nucleation site densities. A very recent complete review on this topic was given by Mori and Utaka[22].

Hu et al.[23,24] were the first to perform LN_2 quenching experiment using a nano-structured surface and proved its feasibility for enhancing heat transfer over the normal surface. This paper reported breakthrough advancements on both fronts of boiling and quenching. The CHF in boiling and the Leidenfrost temperature in quenching are the bottlenecks to the heat transfer advancements. As compared to a conventional aluminum surface, Hu et al.[23,24] reported a substantial enhancement of the CHF by 112% and an increase of the Leidenfrost temperature by 40K using an aluminum surface with anodized aluminum oxide (AAO) nanoporous texture finish. These heat transfer enhancements imply that the power density would increase by more than 100% and the quenching efficiency would be raised by 33%. The heat transfer modification and enhancement were attributed to the superhydrophilic surface property and excessive nanoscale nucleation sites.

Based on the above, it is believed that for the nanoporous surface textures that facilitate the formation of an effective thin low-thermal conductivity surface layer, the enhancement in heat transfer rates is accomplished by the rapid lowering of the surface temperature during initial transient quenching process that shortens the duration of film boiling such that much higher heat transfer regimes of transition and nucleate boiling would take over earlier to achieve the shorter quenching times. Based on this physical concept, it is proposed to use a thin low-thermal conductivity coating layer to take the place of the nanoporous layer for the same enhancement effects.

1.5. Theoretical basis of current experiment

A simple mathematical model was developed based on the theory of transient one-

dimensional conduction in a thin solid slab[25] to illustrate the heat transfer effect of a low-thermal conductivity surface coating. By neglecting the curvature effects, a thin tube wall can be approximated as a thin slab. As shown in Figure 2, the tube walls without and with a surface coating layer are depicted in Figures 2(a) and 2(b), respectively. In Figure 2, T_i and T_f are the slab initial temperature and bulk temperature of the quenching flow, respectively, *h* is the quenching convective heat transfer coefficient between the flow and the surface, α_{ss} and α_c are the thermal diffusivities of stainless steel (original bare tube surface material) and Teflon coating material, respectively, and K_{ss} and K_c are thermal conductivities of stainless steel and Teflon coating material, respectively. More details for the Teflon coating are given later. Based on an approximation method that assumes a small heat diffusion penetration depth for the short initial instance, the solution of the transient one-dimensional conduction in a semi-infinite medium[25] was used. If we only retain the dominant orders, at a small time t after the quenching is initiated, the transient tube surface temperatures of the non-coated stainless steel tube, $T_{S,NC}(t)$ and the Teflon coated tube, $T_{S,C}(t)$ can be shown as follows.

$$\frac{\left(\frac{T_i - T_{S,C}(t)}{T_i - T_f}\right)}{\left(\frac{T_i - T_{S,\mathrm{NC}}(t)}{T_i - T_f}\right)} = \frac{\frac{2}{\sqrt{\pi}}\left(\frac{h\sqrt{\alpha_c t}}{k_c}\right)}{\frac{2}{\sqrt{\pi}}\left(\frac{h\sqrt{\alpha_{ss} t}}{k_{ss}}\right)} = \left(\frac{\alpha_c}{\alpha_{ss}}\right)^{1/2}\left(\frac{k_{ss}}{k_c}\right) \tag{1}$$

After plugging in the thermal properties for both stainless steel and Teflon in the above equation, respectively,

$$\frac{T_i - T_{S,C}(t)}{T_i - T_{S,\mathrm{NC}}(t)} = (0.4)^{\frac{1}{2}}(76.4) = 15.3 \tag{2}$$

Even though Eq. (1) indicates that both ratios of thermal diffusivities and thermal conductivities are involved, but Eq. (2) clearly demonstrates that the thermal conductivity ratio dominates the transient process such that the low thermal conductivity coating can facilitate more than an order of magnitude larger drop of the tube wall surface temperature for the same small elapsed after the quenching is initiated.

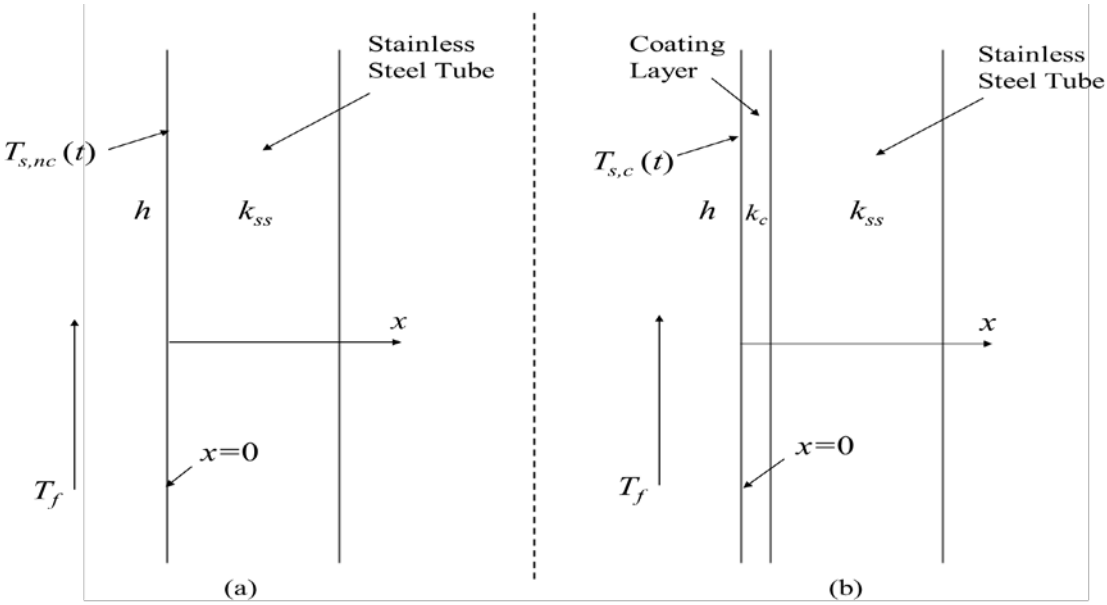

Figure 2. Schematic of transient one-dimensional conduction model.

1.6. Research objective

The primary objective of the current set of experiments was to obtain transient metal tube temperature history curves, or chilldown curves, from room temperature to LN_2 saturation temperatures during quenching on a horizontally-aligned, commercially available 304 stainless steel tube coated with low thermal conductivity thin Teflon layers. Tests were carried out with coatings of four different thicknesses over a wide range of test section inlet pressure levels and corresponding mass flow rates. The effectiveness of the various coating thicknesses was evaluated by a comparison of chilldown curves with coatings to those of a bare surface tube.

2. Experimental Methods

2.1. Experimental Apparatus

This experiment system was designed and built in much the same way as the original rig reported in Darr et al.[9,10] and Darr et al.[11]. The current system built with small modifications to the original rig was intended for both terrestrial and microgravity parabolic flight experiments. Pictures of the test apparatus are shown in Darr et al.[11].

A system flow schematic of the experiment is shown in Figure 3. LN_2 was supplied to the system from an 80L double-walled dewar, with a relief valve set at 861 kPa. A gaseous nitrogen (GN_2) cylinder initially at 15 MPa pressurized the dewar to a set value for each test, which ranged between 90 to 830 kPa absolute pressure. Dewar pressure was managed by pressure regulator 1 (PR1), which fixed the dewar pressure to within 35 kPa of the set value during each test. Depressurization was carried out by opening globe valve 1 (GV1) and three-way ball valve 1 (3V1) to allow ullage gas to vent to the atmosphere. Pressurization was carried out by closing ball valve (BV1) and opening BV2 to route flow from the first gas cylinder to the dewar. PR1 was used to regulate the dewar pressure. PR2 was a backup regulator to prevent large pressure spikes. In operation, PR2 was always left fully open to 862 kPa gauge pressure.

The dewar was used both for prechilling the plumbing upstream of the test section and for running the actual chilldown experiment. LN_2 was delivered through a ½" nominal inner diameter (ID) globe valve (GV2). GV2 was connected, through a 1.2 m long, 1.27 cm outer diameter (OD), 1.18 cm ID 304SS braided hose to the inner tube of a "subcooler". Further details of the subcooler are given in Darr et al.[9] The purpose of the subcooler was to insulate the tubing upstream of the test section so that the fluid entering the test section was vapor free, subcooled liquid.

During the prechilling process, the liquid exiting the inner tube of the subcooler was directed by two “T-type” 316SS ½” ID three-way ball valves (3V3 and 3V2) to a fill-port on top of the outer vessel of the subcooler. A 3 cm long, 1.270 cm OD, 1.168 cm ID 304SS tube connected 3V3 and the subcooler. The fill port and vent port of the subcooler were switched from the original experiment. A 2.5 cm ID port allowed evaporating liquid to escape the subcooler. The fluid was directed to an electrically heated “vaporizer” Vap1 which vaporized any entrained liquid and warmed the vapor above 273 K before entering the atmosphere. A pressure transducer (PT) and TC, labeled “Inlet PT, TC” in the schematic, were connected at a distance of 7 cm from the downstream side of the inner tube of the subcooler to measure a fluid pressure and fluid temperature near the inlet of the test section, which determined the level of inlet subcooling for each test.

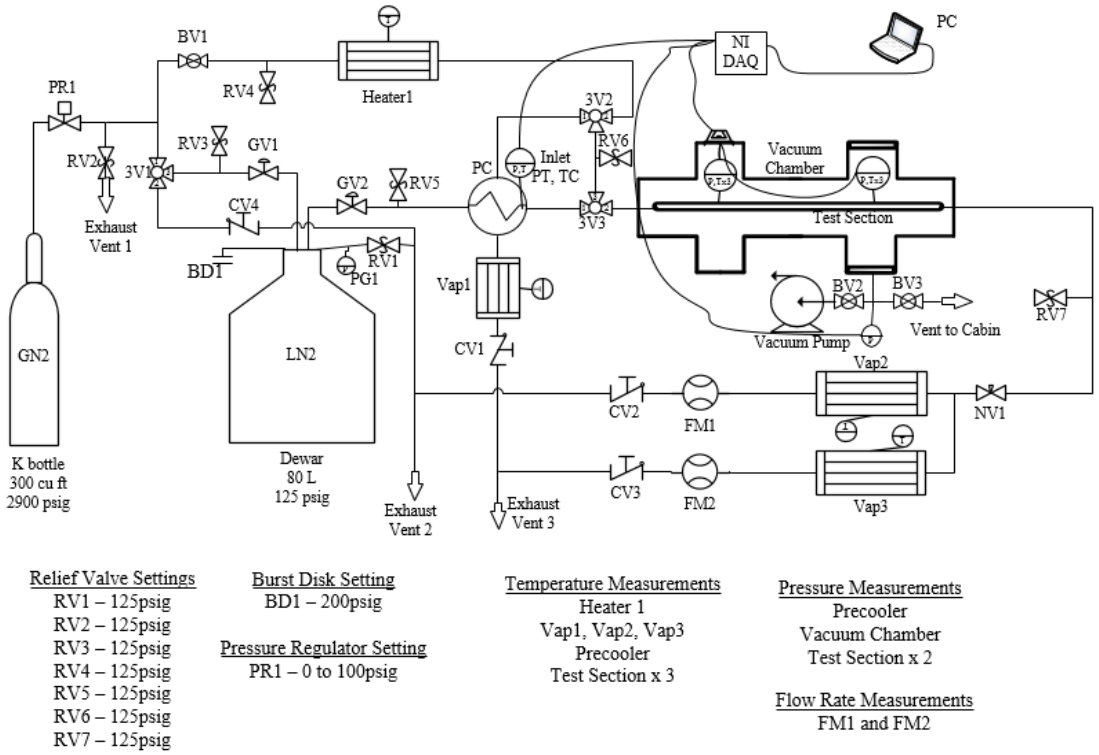

Figure 3. Schematic of the experimental flow system

Once this temperature measurement reached a steady value, and the temperature was below the saturation temperature based on the measured pressure, a chilldown test could begin. To start a test, 3V3 was turned so that flow was directed to the test section instead of the subcooler fill port. The valve was manually operated during the experiment. Flow entering 3V3 would turn 90° towards 3V2 during the subcooling operation, or it would travel straight through to flow into the test section. The subcooler and test section were connected to the rig so that they were parallel to the floor, in a horizontal flow configuration. Two layers of 6.35 mm thick aerogel insulation were wrapped around GV2, the hose upstream of the subcooler, the subcooler itself, 3V3, and the 3 cm length of tube between 3V3 and the subcooler to minimize heat leak into the system upstream of the test section.

As shown in Figure 4, the test section was a 57.2 cm long, 1.270 cm OD, 1.168 cm ID 304SS tube. A length of 2.54 cm of the test section tube protruded out of each side of the vacuum chamber. Six TCs were soldered to the outside of the tube, with three placed an axial distance of 14.9 cm from the test section inlet (upstream TC station), and three placed 40.1 cm from the inlet (downstream TC station). As detailed in Figure 4, for each station, the TCs were spaced out radially in 90° increments such that each station had a top, side, and bottom TC. Two cryogenic rated PTs were connected to two short pieces of 304SS tube protruding perpendicularly from the test section, one near each TC station. These tubes were welded to the test section.

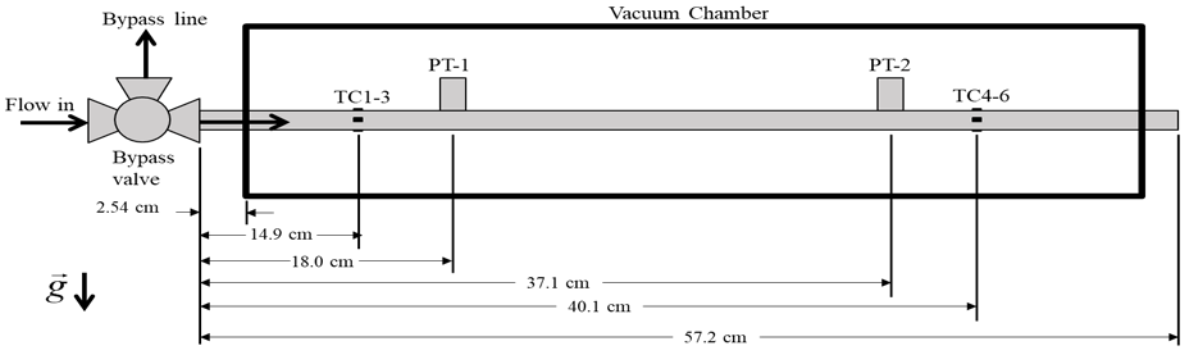

(a)

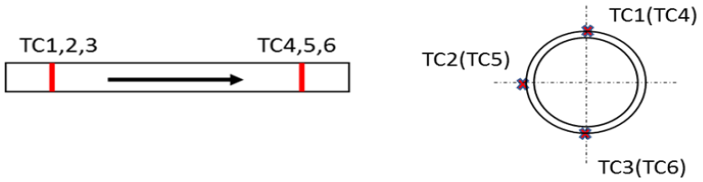

(b)

Figure 4. Test section dimensions.

The 316SS vacuum chamber that housed the test section was the same as the original experiment. The purpose of the vacuum chamber was to reduce parasitic heat leak which reduced the uncertainty in the calculation of wall-to-fluid heat flux. A diaphragm pump and molecular turbopump were used to bring the air pressure surrounding the test section to approximately 1 Pa. This reduced the parasitic heat leak due to conduction between the test section and the air inside the vacuum chamber to less than 10% of the lowest measured convective heat flux, which occurred during film boiling at the lowest flow rate that was tested. Parasitic heat leak was less than 1% of the measured value for most of the data points.

The needle valve downstream of the test section (NV1) was throttled at three different positions so that tests could be run at different flow rates for the same dewar pressure setting. The flow was routed from the needle valve by a SS tube to two separate pipes (labeled Vap2 and Vap3) that were electrically heated to vaporize the flow. To enhance the heat transfer, eight 1.27 cm OD copper tubes were packed inside each pipe in an octaweb configuration. One electrical heating tape was wrapped around each pipe to heat it to 480 K before each test. A TC was placed on the outer surface of each heat tape to monitor the temperature in real time. The flow out of Vap2 and Vap3 entered two separate, identical gas flow meters (FM1 and FM2) that each had a capacity of 4000 standard liters per minute. The flow was then directed to the vent ports.

The test was completed when the test section TC measurements read a steady state temperature below the saturation temperature based on the test section PT readings. At this time, the

liquid-delivery valve on the dewar, GV2, was closed to prevent liquid flow from the dewar. Before running the next test, the test section was quickly heated up by opening BV1 and turning 3V1 and 3V2 to allow warm gas flow from the gas cylinder to enter the test section. Once the dewar was pressurized and the test section was heated to room temperature, the next test was ready to begin with the subcooling process. A data acquisition unit collected all sensor data and displayed it real-time on a laptop computer connected to the rig. All TCs were T-type and were measured at a frequency of 15 Hz. Hz. The Flow meter and PT were running at 2 Hz and 80 Hz, respectively.

2.2. Experimental procedure

The tests were operated as follows: At the start, the needle valve was set to the target position for the given test, Vap 1, Vap2, and Vap3 were heated up to 480 K, and the vacuum pump system was turned on. The total time from starting the pump to reaching 1 Pa inside the vacuum chamber took roughly 15 minutes. Concurrently, the inner tube inside the subcooler was chilled by pressurizing the dewar, opening GV2, and directing the flow through 3V3 and 3V2 to the fill port of the subcooler. The subcooler took approximately 10 minutes to completely chill and fill. Then, 3V2 was shut off from the flow from 3V3, and the dewar was pressurized by opening PR1 to the desired dewar gauge pressure. Pressurization was done as quickly as possible before the liquid inside the dewar could warm to the saturation temperature at the new dewar pressure, and also before the liquid inside the plumbing upstream of the test section could gain enough heat to start boiling. Shortly after, 3V3 was turned to start the flow into the test section. Once the TC readings dropped to or below the saturation temperature and maintained a steady temperature, GV2 was closed. This marked the end of the test. In preparation for the next test, Heater 1 was turned on and 3V2 and 3V3 were rearranged so that warm gas entered the test section to carry out the reheat process. After

reheating was finished, NV1 was set at the new position. Vap2 and Vap3 were allowed to heat up to above 480 K, and the subcooling process was repeated to account for the lost LN_2.

2.3. Experimental uncertainties

As mentioned above, the current experimental system is virtually identical to that employed in Darr et al. [9,10], the readers are referred to Darr et al.[9,10] for uncertainties on those independent, directly measured quantities, such as temperatures and pressures.

2.4. Coating of tube inner surface

In the current experiment, the stainless steel test tube was coated with low-thermal conductivity thin Teflon layers on the inner surface. Specifically, the coating material was made of Fluorinated Ethylene Propylene (FEP) by DuPont and classified by DuPont as Teflon 959G-203 that is a black color paint and has a thermal conductivity of 0.195 W/mK (DuPont publication[26]). The coating was put on by the Matrix Coating Corporation (West Palm Beach, FL 33404, USA) using the pour and drain process. The final thickness of the coating on the tube depends on the number of layers processed. After each pour and drain, the fresh film layer was cured in a furnace through a standard sintering procedure before adding another layer by the same pour and drain procedure. As a result, the final thickness of coated layer depends on the total number of layers processed.

Twenty-four coated tubes were made with four different final layer thicknesses that are identified as one-layer (1L), two-layer (2L), three-layer (3L), and four-layer (4L) coatings. For example, the 4L coating went through the pour and drain process four separate times. To determine the coating layer thickness, high resolution computer tomography (CT) x-ray scans of the tube cross sections were obtained using a Phoenix v|tome|x M (GE's Measurement & Control business, Boston, USA) system in the Nano Research Facility at the University of Florida. Scanning was carried out using a 240 kV X-ray tube and a tungsten on beryllium target, with the following settings: 200 kV,

50 milliamps, and 0.5 mm Tin filter. Images were collected from 1600 pixels horizontal, 2024 pixels vertical, 0.5 s detector exposure, averaging of 4 images per rotation position with a one-exposure skip and a total of 2200 rotational positions. The average thickness and uncertainty for each of the four coating layers are provided in Table 1.

Table 1. Total coating layer thickness for the four types.

Coating Type	1L	2L	3L	4L
Total Thickness	$15.33 \pm 0.6\ \mu m$	$25.8 \pm 0.7\ \mu m$	$45.28 \pm 0.7\ \mu m$	$64.8 \pm 0.7\ \mu$m

3. Results and Discussion

Five tubes with four different inner surface modifications (bare surface without coating, 1L, 2L, 3L, and 4L) were tested at six different LN_2 mass flow rates that corresponded to inlet pressures of 100 psig, 80 psig, 60 psig, 40 psig, 30 psig and 20 psig, respectively. From the 30 chilldown tests that were performed for evaluating the effects of various coating thicknesses, 25 cases as listed in Table 2 were selected for presenting the results, comparison, and discussion. Table 2 lists the average mass flux, G_{ave} and the Reynolds number based on the average mass flux.

Table 2. Conditions for three of the 54 tests, representing low flow rate, medium flow rate, and high flow rate tests. Conditions are based on the upstream TC station.

Case	Coating Applied	P_{in} psig	Re_{ave}	G_{ave}, kg/m^{2}s
1	No Coating	100	63,178	2,362
2	No Coating	80	50,733	2,057
3	No Coating	60	40,657	1,828
4	No Coating	40	33,774	1,687
5	No Coating	20	19,506	1,160
6	1L Coating	100	111,341	4,243
7	1L Coating	80	79,354	3,239
8	1L Coating	60	56,102	2,468
9	1L Coating	40	46,833	2,312
10	1L Coating	20	23,537	1,346
11	2L Coating	100	91,612	3,354
12	2L Coating	80	73,934	2,943
13	2L Coating	60	56,031	2,480
14	2L Coating	40	37,362	1,866
15	2L Coating	20	21,209	1,231

16	3L Coating	100	102,858	3,898
17	3L Coating	80	79,951	3,198
18	3L Coating	60	63,178	2,742
19	3L Coating	40	45,127	2,205
20	3L Coating	20	19,072	1,119
21	4L Coating	100	98,803	3,690
22	4L Coating	80	68,047	2,764
23	4L Coating	60	59,210	2,584
24	4L Coating	40	40,785	1,982
25	4L Coating	20	15,924	952

3.1. Typical chilldown curve and boiling curve

Before we present and discuss the effects of coating on the quenching of a metal tube, the physics and characteristics of the tube quenching process must be clearly explained first. Figure 5 and Figure 6 show the typical chilldown curves and boiling curves, respectively, for Case 1 which is considered the baseline case. The chilldown curves provides the tube wall outer surface temperature histories during chilldown at both upstream and downstream locations from the tube inlet. It is noted that the outer wall surface temperature is the maximum and that of the inner surface is the minimum for any axial location during chilldown. Therefore, the chilldown is complete when the outer wall surface temperature has reached the liquid saturation temperature. As shown in Figure 5, six chilldown curves were plotted using the temperature data registered by the six thermocouples (TCs) shown in Figure 4(b), where TCs 1(top), 2(side) and 3(bottom) are located in the upstream station and TCs 4(top), 5(side) and 6(bottom) are located in the downstream station. In general, all six chilldown curves display similar trends where the heat transfer process during cooling of the tube went through film, transition and nucleate boiling regimes, sequentially as explained in Figure 1 and also next by the boiling curve (Figure 6). At a specific TC station, the chilldown time is the shortest for the bottom location, second shortest for the side, and longest for the top. However, for the same circumferential location at a TC station, the downstream one lagged behind that in the upstream

station due to the fact it takes more time for the cooling fluid to reach the downstream location. However, it should be pointed out that the downstream ones actually started to lower their temperatures at the same time as the upstream ones but at slower rates due to cooling by the axial conduction heat transfer in the metal tube wall.

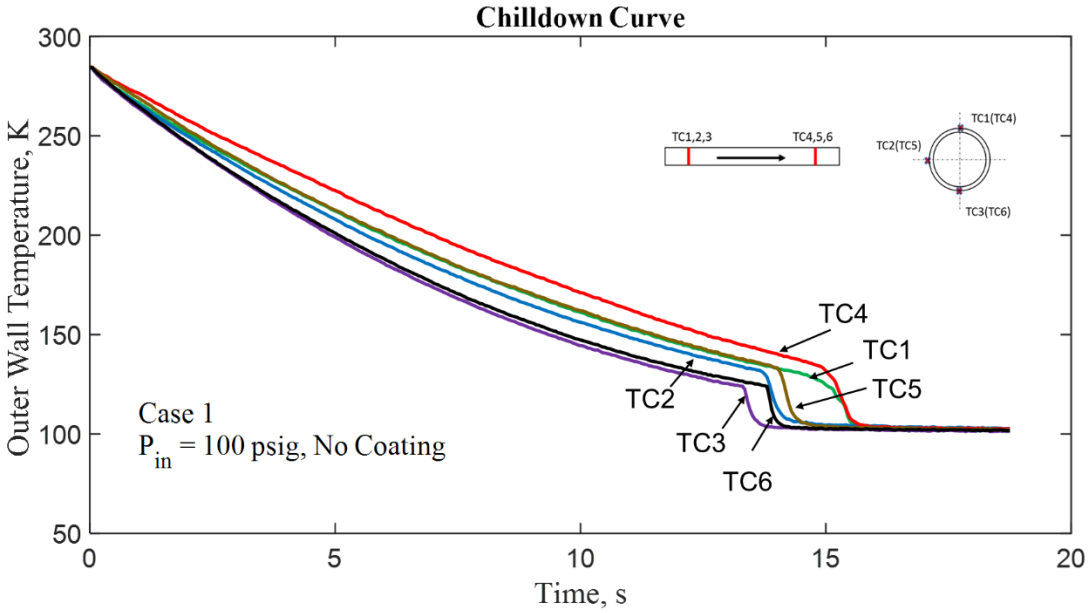

Figure 5. Tube wall outer surface temperature vs. time (chilldown curve) at each of the 6 TC locations for an inlet pressure of 100psig (Case 1).

Figure 6(b) shows the so-called "boiling curve" for the bottom location (TC3) at the upstream TC station for Case 1. A boiling curve illustrates the heat transfer characteristics during chilldown by providing the inner wall transient surface heat flux as a function of inner wall surface temperature. Together, the corresponding chilldown curve and boiling curve in Figures 6(a) and 6(b), respectively, share the common surface temperature scale. The boiling curve shows the heat transfer regimes, Leidenfrost point (LFP) and CHF point as a function of surface temperature. As indicated in Fig. 1, film boiling takes place from the start to the LFP, followed by transition boiling between the LFP and the CHF point. Nucleate boiling ensues after the CHF point. As can be seen in Figure 6, for LN_2 chilldown, the majority of time is spent in the film boiling regime. After the rewetting

(LFP), the heat fluxes are much higher in the transition regime and nucleate boiling regime that results in the rapid cooling of the tube wall and a corresponding sudden increase in the slope of the chilldown curve. As shown in Fig. 5(a), the LFP is located just ahead of the sharp turn of the chilldown curve, and the almost vertical line corresponds to the transition and nucleate boiling regimes with the CHF separating the two regimes. For the current Case 1, the film boiling regime lasted 12.8 seconds. The transition and nucleate boiling together lasted about 0.5-1s, after which single-phase liquid convection heat transfer persists at low heat fluxes. The main reason for this elapsed time difference is that the film boiling heat fluxes are much smaller than those in transitional and nucleate boiling.

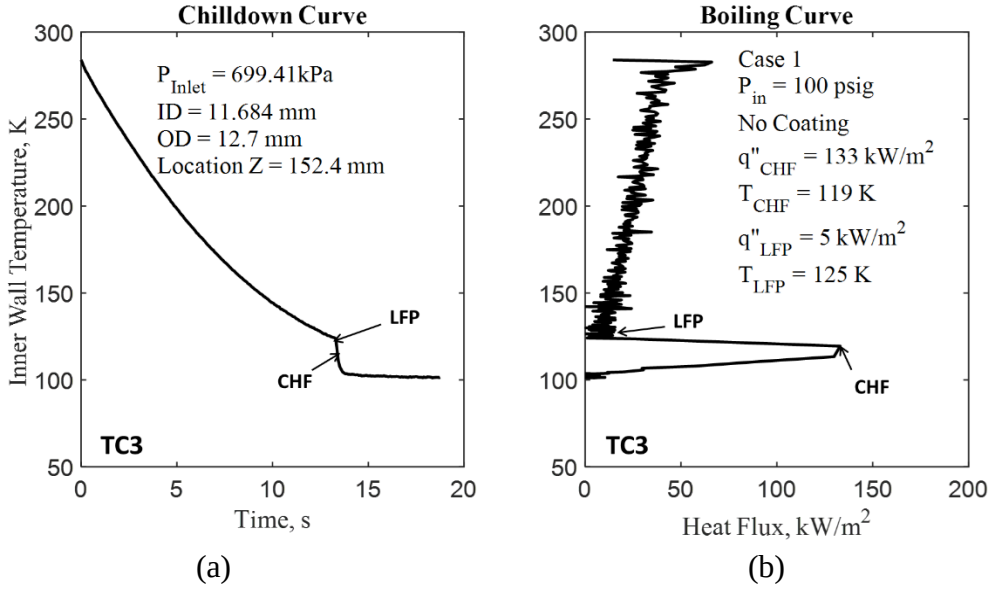

Figure 6. (a) computed inner wall temperature vs. time at TC3. (b) heat flux vs. time (boiling curve) at TC3, both for Case 1.

It is also noted that the rewetting (LFP) temperature, T_{wet}, is 125K which is 155K lower than the initial wall temperature of 280K. The chilldown and boiling curves, while as a representative example to show the general trends, can change depending on the fluid type, flow rate, pressure, flow direction, axial location along the pipe, and the pipe diameter.

3.2. The coating effects on chilldown times

The effects of four different coating thicknesses (1L, 2L, 3L, and 4L) on the chilldown process are presented in Figures 7(a)-(d) for an inlet pressure of 100 psig. For each figure, the five chilldown curves that correspond to four coating thicknesses and one bare surface without a coating are plotted. Figures 7(a) and 7(b) show data for TC1 and TC3, respectively. Figures 7(c) and 7(d) show data for TC4 and TC6, respectively. The following observations on the effects of coating thickness were made from these figures. Note that similar trends and results were found for the two side thermocouples, TC2 and TC5, therefore they are not shown here.

1. It is clear that the reduction in chilldown time is directly related to the number of coating layers. More layers produce shorter chilldown time results.
2. For the upstream station, chilldown times are relatively closer between 2L and 3L tubes while for the downstream station, the chilldown times are relatively closer between 3L and 4L tubes.
3. The film boiling regimes are almost eliminated in 4L tube for TC3, TC4, and TC6 locations.

Next, performace of the coating layers is examined for various inlet pressures that corresponds to different mass flow rates as indicated in Table 2 . Figures 8(a) and 8(b) plot the results for TC1 at the upstream station where chilldown curves are shown for 0L, 1L, and 4L tubes under 100 psig, 60 psig, 40 psig, and 20 psig. Figures 8(c) and 8(d) plot the results for TC4 at the downstream station where chilldown curves are also given for 0L, 1L, and 4L tubes under 100 psig, 60 psig, 40 psig, and 20 psig.

The general assessment of the coating layer performances for different inlet pressures is given as follows.

1. The consistent trend demonstrates that for a given coating layer thickness, the higher the inlet pressure is, the shorter the chilldown time is required. This outcome is basically due

the fact that a higher inlet pressure facilitates a higher mass flow rate that gives rise to higher cooling rates. This is an improvement of some other boiling heat transfer enhancement methods that become less effective at high fluid velocities as convection dominates over local boiling heat transfer.

2. For a given inlet pressure, the results conform to the trends given above for the effect of coating layer thickness under a constant inlet pressure.

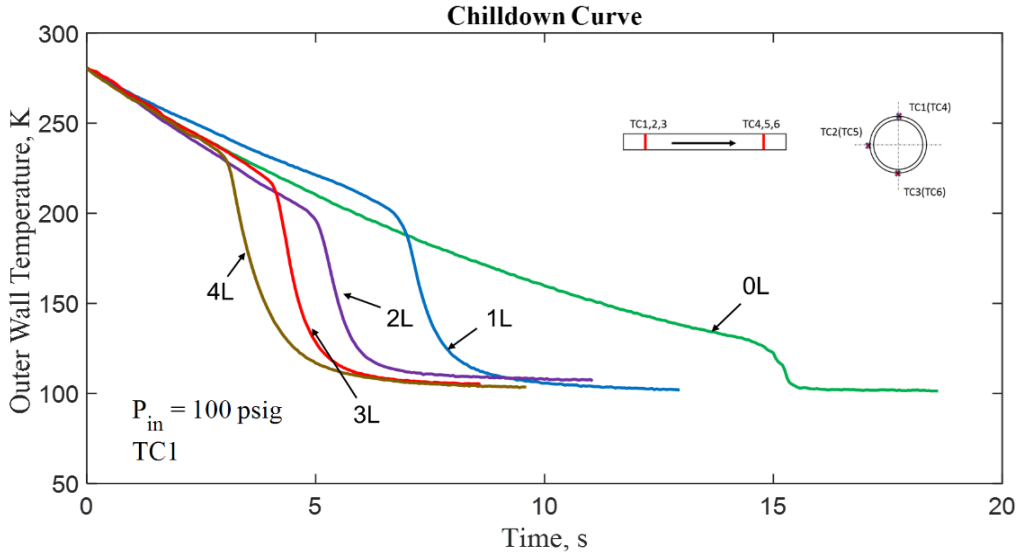

(a)

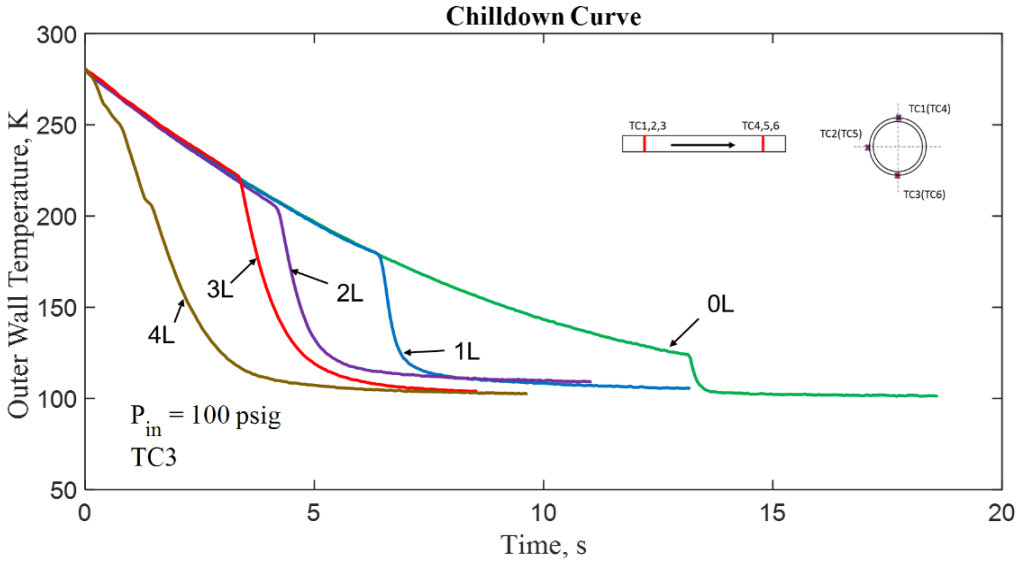

(b)

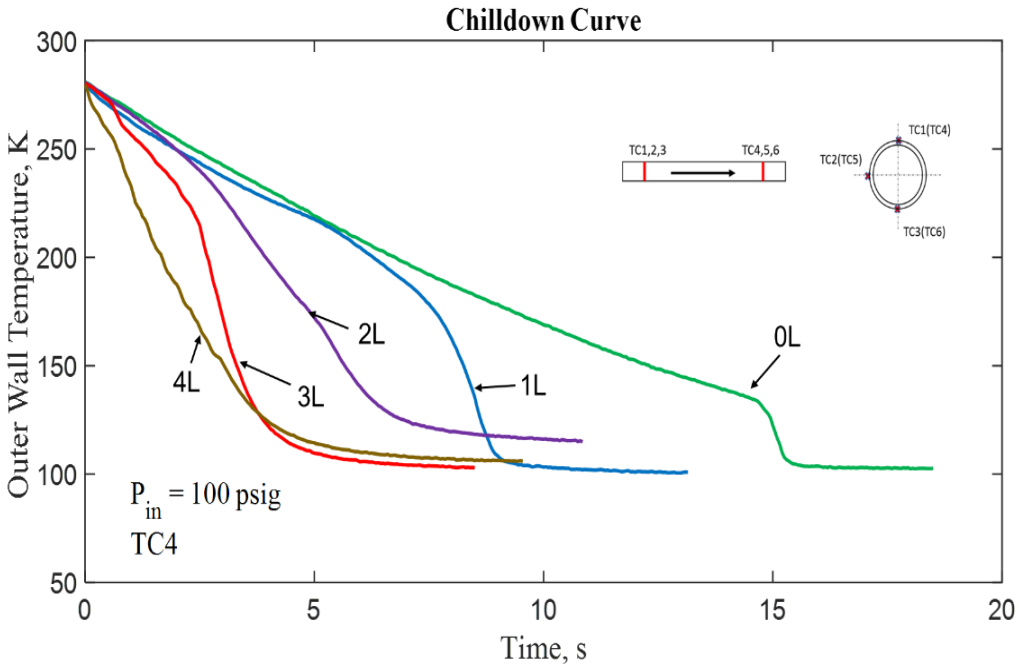

(c)

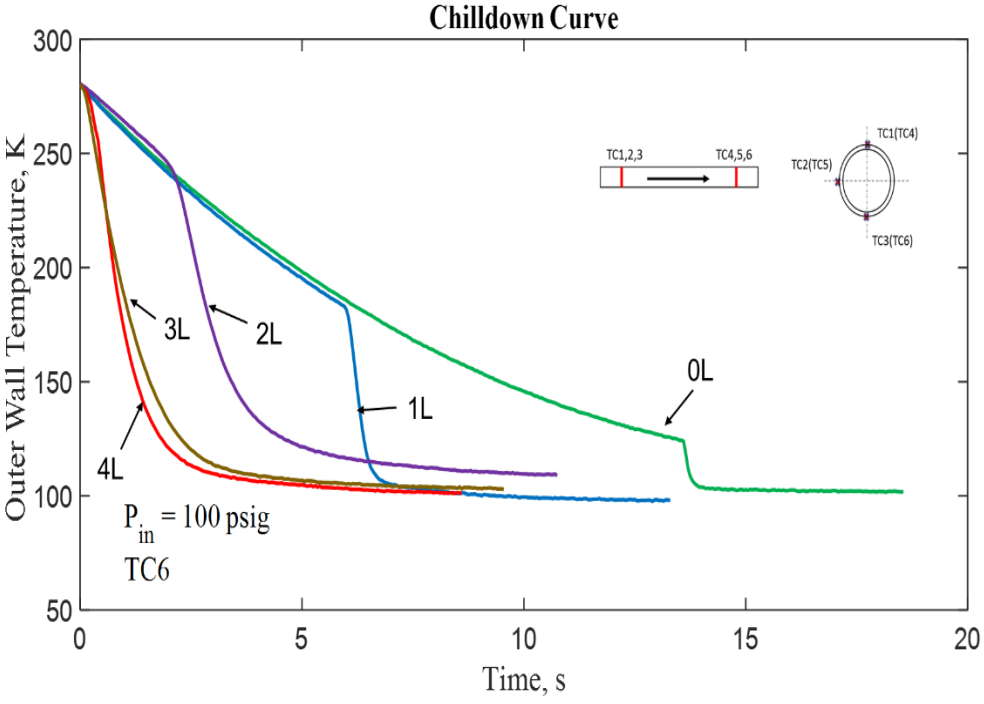

(d)

Figure 7. Chilldown curves for different coating layers at an inlet pressure of 100psig. (a) TC1 – top of the tube, upstream. (b) TC3 – bottom of the tube, upstream. (c) TC4 – top of the tube, downstream. (d) TC6 – bottom of the tube, downstream.

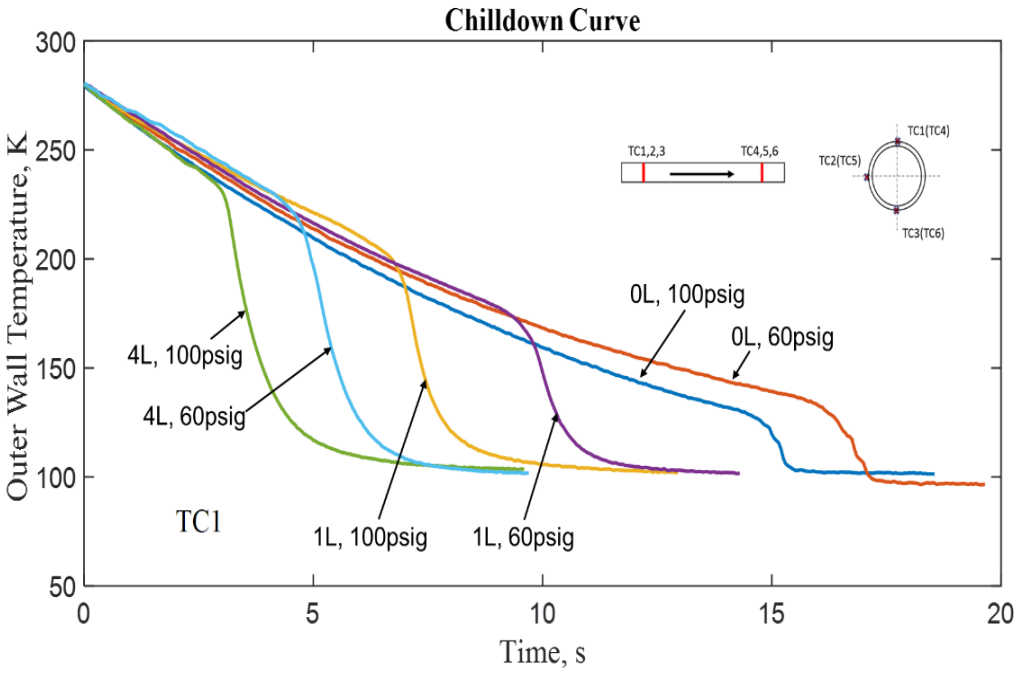
Chilldown Curve
Outer Wall Temperature, K
Time, s
TC1,2,3
TC4,5,6
TC1(TC4)
TC2(TC5)
TC3(TC6)
0L, 100psig
0L, 60psig
4L, 100psig
4L, 60psig
TC1
1L, 100psig
1L, 60psig

(a)

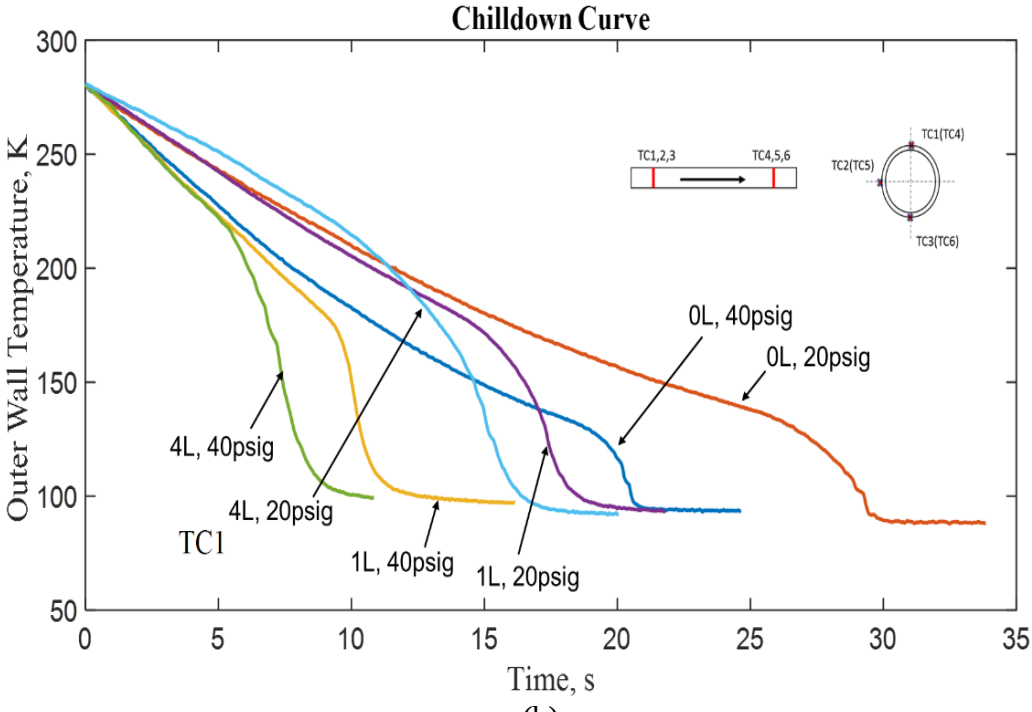
Chilldown Curve
Outer Wall Temperature, K
Time, s
TC1,2,3
TC4,5,6
TC1(TC4)
TC2(TC5)
TC3(TC6)
0L, 40psig
0L, 20psig
4L, 40psig
4L, 20psig
TC1
1L, 40psig
1L, 20psig

(b)

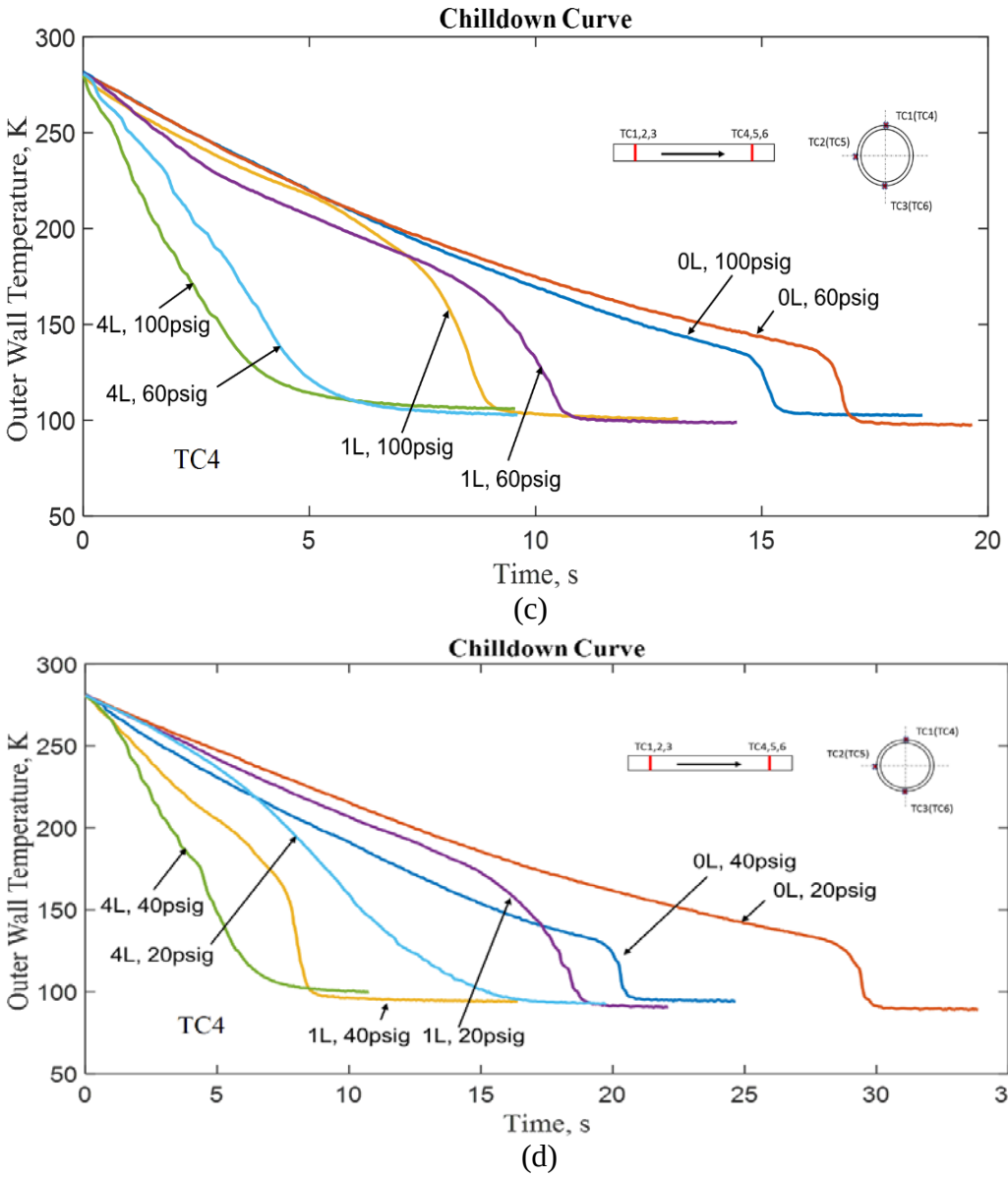

Figure 8. Chilldown curves at different pressures for 0L, 1L, and 4L coatings. (a) TC1 at 100psig and 60psig inlet pressures. (b) TC1 at 40psig and 20psig inlet pressures. (c) TC4 at 100psig and 60psig inlet pressures. (d) TC4 at 40psig and 20psig inlet pressures.

3.3. The coating effects on boiling characteristics

3.3.1. The rewetting (LFP) temperature and the heat flux at the LFP

Further explanation of the physics of chilldown results for different coating layer thicknesses is facilitated by the plots of boiling curves that show the changes of the boiling regimes, LFP,

and CHF. Figures 9(a), (b), and (c) are plots of boiling curves from data collected by TC6 for inlet pressures of 100 psig, 60 psig, and 20 psig, respectively. The key findings are listed below.

1. For inlet pressure at 100 psig, the LFP temperature is raised from 124k to 180K when 1L tube was used versus the bare tube (0L). The Leidenfrost temperature increase to 263K psia
2. when the 4L tube was used. Similarly, for 60 psig inlet pressure, the Leidenfrost temperatures are 123K, 180K, and 261K when using 0L, 1L, and 4L tubes, respectively. Lastly, for 20 psig inlet pressure, the Leidenfrost temperatures are 118K, 171K, and 264K when using 0L, 1L, and 4L tubes, respectively. It appears that the changes on the LFP temperature are a function of the coating layer thickness and not sensitive to the inlet pressure or mass flow rate. A higher LFP temperature shortens the film boiling period that contributes to a faster chilldown time.
3. The coatings have been found to increase the heat flux levels at the LFP, q''_{LFP}. At 100 psig inlet pressure, the q''_{LFP} values are 4 kW/m^2, 15 kW/m^2, and 39 kW/m^2 when 0L, 1L, and 4L tubes were used, respectively. The q''_{LFP} values are 6 kW/m^2, 10 kW/m^2, and 37 kW/m^2 for 60 psig inlet pressure, and 6 kW/m^2, 8 kW/m^2, and 28 kW/m^2 for 20 psig inlet pressure, when 0L, 1L, and 4L tubes were used, respectively.
4. For all three pressures, as a result of the increases on the LFP temperatures, the time spent on the film boiling regime is shortened. For example, at 100 psig inlet pressure, the film boiling periods were 13.8s, 6.5s, and 0.5s for 0L, 1l, and 4L tubes, respectively. Similar trends were seen for other inlet pressures. Of most significance is that for all three inlet pressures, the inefficient film boiling are almost completely eliminated for the 4L tube.

5. The above findings, resuts and trends can be applied to other TCs and inlet pressures investigated in the current paper.

3.3.2. CHF and temperature at CHF

In this section, we focus on the CHF, q''_{CHF}, values and the corresponding CHF point inner wall surface temperatures. The primary findings are listed below based on Figure 9.

1. The coating layers have been found to increase the heat flux levels at CHF point, q''_{CHF}. For example at 100 psig inlet pressure, the q''_{CHF} values are 179 kW/m^2, 269 kW/m^2, and 224 kW/m^2 when 0L, 1L, and 4L tubes were used, respectively. The q''_{CHF} values are 177 kW/m^2, 243 kW/m^2, and 224 kW/m^2 for 60 psig inlet pressure, and 177 kW/m^2, 204 kW/m^2, and 200 kW/m^2 for 20 psig inlet pressure, when 0L, 1L, and 4L tubes were used, respectively. The coatings generally raise the CHF values 23% to 50% over the bare surface tubes.
2. For inlet pressure at 100 psi, the CHF point temperature is raised from 114k to 121K when 1L tube was used versus the bare tube (0L). The CHF temperature goes up to 160K when the 4L tube was used. For 60 psig inlet pressure, the CHF temperature are 109K, 112K, and 149K when using 0L, 1L, and 4L tubes, respectively, that are slightly lower than those at 100 psig inlet pressures. While for 20 psig inlet pressure, the CHF temperatures are 110K, 102K, and 159K when using 0L, 1L, and 4L tubes, respectively, that trend is very close to that for 60 psig inlet pressure.
3. It is clear that the raising of the CHF temperatures by the coatings facilitaes higher CHF and higher wall temperatures at the CHF. As a result, the chilldown takes place mostly under very high nucleate boiling heat transfer rates that is the main reason that the

chilldown times are drastically reduced when the coated tubes were used. For example, the chilldown times are the shortest for 4L tubes as the chilldown took place almost completely under ultra high nucleate boiling heat transfer rates.

4. The above findings, resuts and trends can be applied to other TCs and inlet pressures investigated in the current paper.

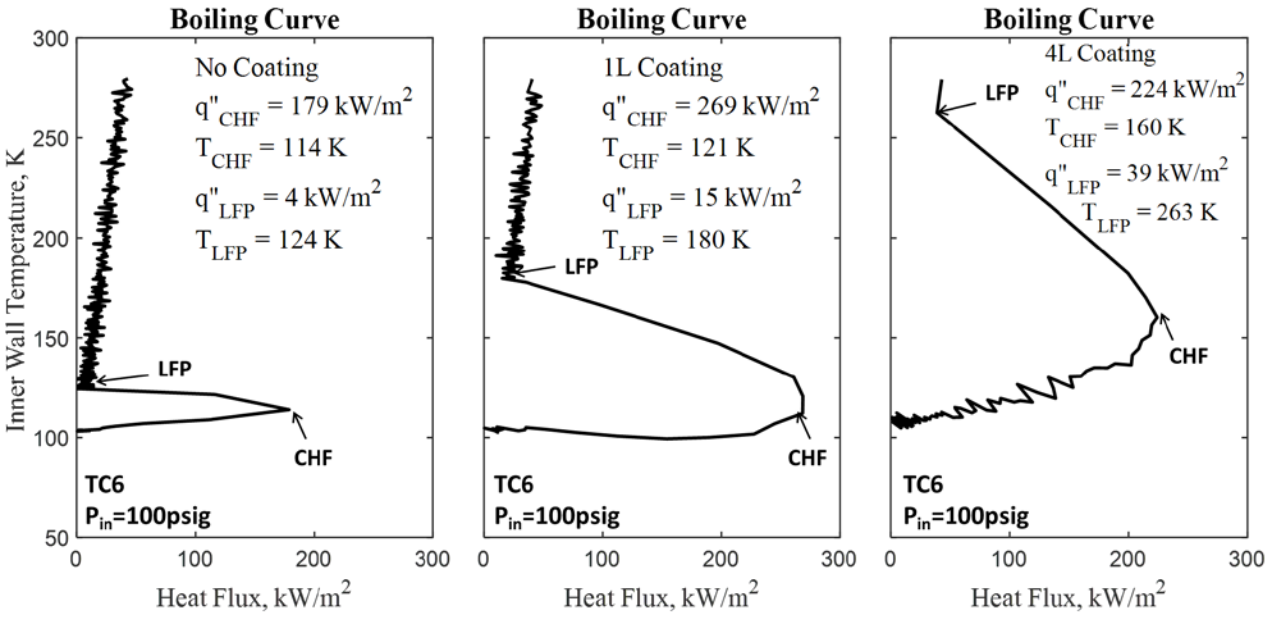

(a)

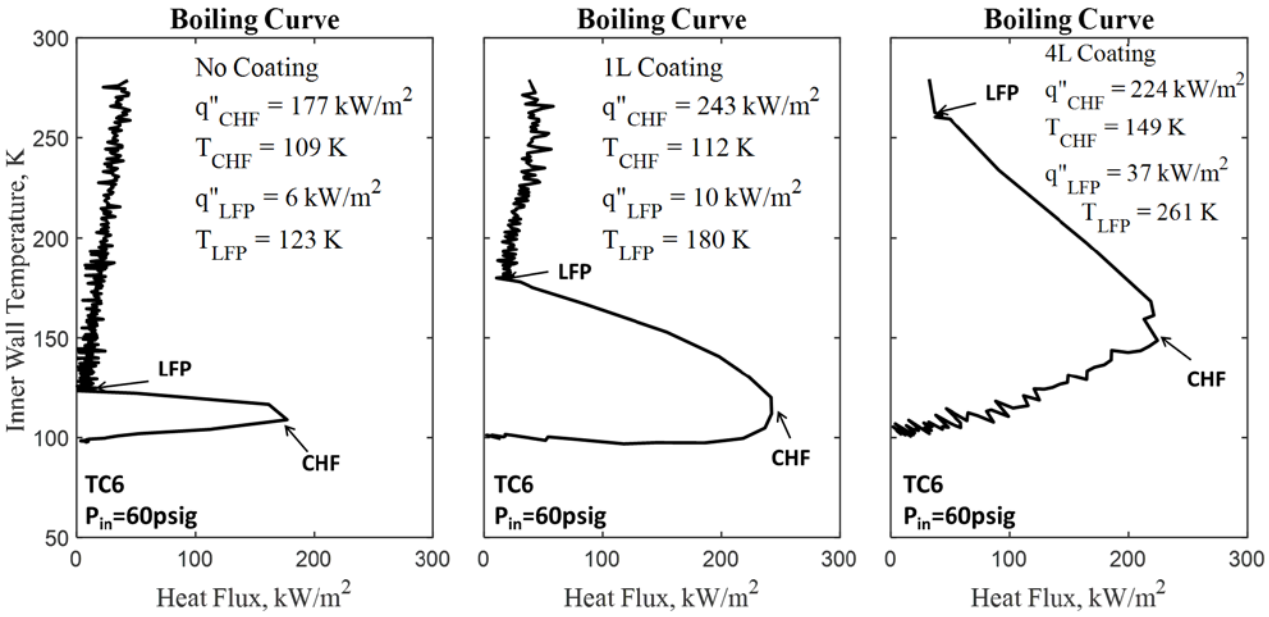

(b)

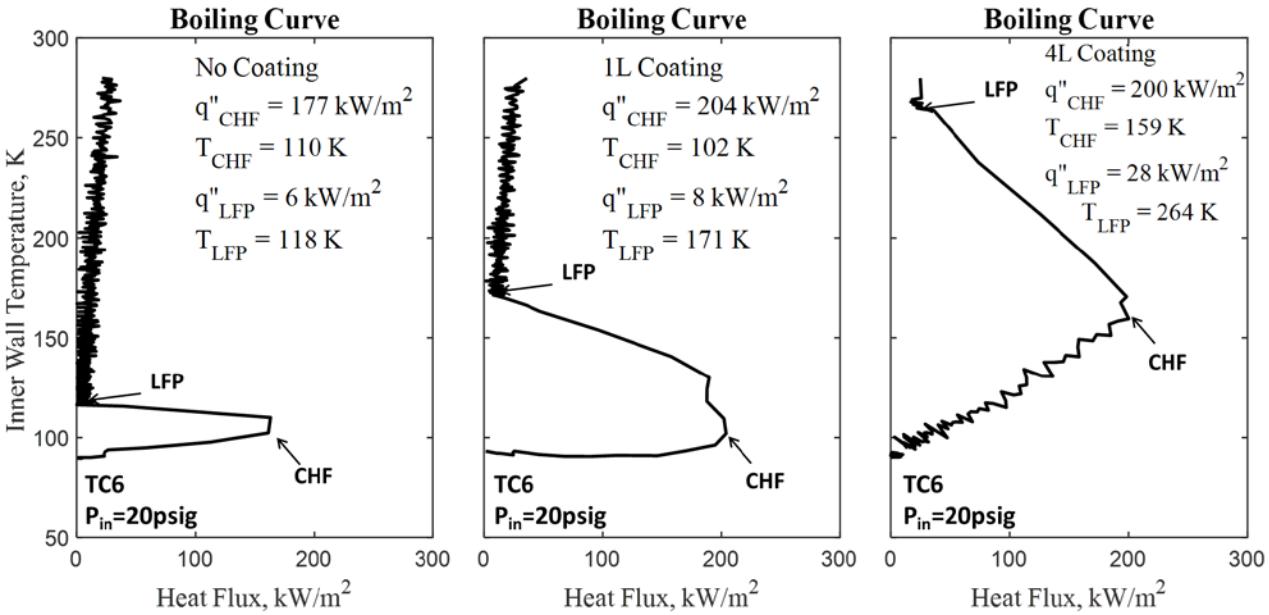

(c)

Figure 9. Boiling curves for different coatings at the T6 location (bottom TC, downstream location). The CHF and Leidenfrost points are included in each plot. For each of (a), (b), and (c), the left plot is for no coating, the middle plot is for a 1L coating, and the right plot is for a 4L coating. (a) Inlet pressure of 100psig. (b) Inlet pressure of 60psig. (c) Inlet pressure of 20psig.

3.4. The effects of coating layers on the enhancement of chilldown efficiency

The chilldown efficiency as defined below represents the percent of total quenching capacity of the cryogent liquid that is actually utilized in lowering the tube wall temperature. The chilldown efficiency, η_{CD}, is therefore defined as,

$$\eta_{CD} = \frac{Q_{\text{Removed}}}{Q_{Comsumed}} \times 100\% \tag{3}$$

In the above, Q_{Removed} is the total thermal energy removed by the cooling fluid during chilldown and is defined as,

$$Q_w = \left(M_{tube} + 0.3M_{valve}\right) c_{p,SS} \left(T_{initial} - T_{final}\right) \tag{4}$$

Where M_{tube} and M_{valve} are the mass of the tube section and that of the three-way globe bypass valve (shown in Figure 2), respectively. A factor of 0.3 is applied to the valve mass, as it is estimated that only 30% of the valve mass needs to be chilldown when the valve is opened and the chilldown starts, since part of the valve is in contact with the LN_2 before the opening of the valve. Therefore, the valve is partially chilled during precooling and reheating of the test section where the LN_2 fills the path all the way to the valve. $c_{P,SS}$ is the stainless steel specific heat for both the tube and valve materials. $T_{Initial}$ and T_{Final} are the initial temperature and the final temperature when the chilldown is completed, respectively. The end of chilldown temperature is the liquid saturation temperature corresponding to the local pressure. $Q_{Consumed}$ is the total quenching capability available during the chilldown process. It is defined as,

$$Q_{Consumed} = M_{coolant} h_{fg} \tag{5}$$

Where $M_{Coolant}$ is the total mass of coolant used and it can be estimated as,

$$M_{Coolant} = \int_0^{t_{End}} \dot{m}(t)dt \tag{6}$$

$\dot{m}(t)$ is the recorded time-dependent coolant mass flow rate and t_{End} is the end of chilldown time. Therefore, $M_{Coolant}$ is the total mass of cryogenic coolant consumed in the entire chilldown process. h_{fg} is the latent heat of vaporization per unit mass that means $Q_{Consumed}$ is the total quenching capability consumed during the chilldown process. The chilldown efficiencies for various source pressures and different coating thicknesses (0L, 1L, 2L, 3L and 4L) are provided in Table 3. First, for the bare surface case, the chilldown efficiencies do not seem to be affected by the variation of the source pressure as the efficiencies fluctuated around 40% for the four inlet pressures. It should be noted that the percent uncertainties for the chilldown efficiency are about 14% (Table 6 below). An important finding is that for the effects of the coating layers, the efficiency increases with increasing number of layers. However, the efficiency increases with decreasing inlet pressure level. In general, the efficiencies cover a range between 38.3% and 80%. To illustrate this, a definition for the percent increase in efficiency over the non-coated case is given as follows and the results are also given in Table 4.

$$\text{Percentage Increase in Efficiency} = \frac{\eta_{xL} - \eta_{0L}}{\eta_{0L}} \times 100\% \tag{7}$$

For the percentage increase in the efficiency, the minimum is 4.2% for 1L and 80 psig inlet pressure and the maximum is 109.1% for 4L and 20 psig inlet pressure. As given above, the total LN_2 consumed in a chilldown process is $M_{coolant}$ and the percent reduction in LN_2 consumption for xL coating is defined below.

$$\text{Percentage Reduction in Mass for xL} = \frac{M_{coolant,0L} - M_{coolant,xL}}{M_{coolant,xL}} \times 100\% \tag{8}$$

Table 3. The chilldown efficiencies, η_{CD}, for different coating layers and the percentage increase in η_{CD} over the base case, 0L.

P_{in} (psig)		0L	1L	2L	3L	4L
80	η_{CD}(%)	40.6	42.3	47.5	54.0	47.7
	Percent increase in η_{CD}(%)	0	4.2	17.2	33.0	17.5
60	η_{CD}(%)	42.3	46.8	52.6	59.3	64.0
	Percent increase in η_{CD}(%)	0	10.5	24.4	40.1	51.3
40	η_{CD}(%)	37.5	56.1	63.6	62.2	70.3
	Percent increase in η_{CD}(%)	0	49.7	69.7	66.1	87.6
20	η_{CD}(%)	38.3	49.7	59.5	70.8	80.0
	Percent increase in η_{CD}(%)	0	30.0	55.5	85.0	109.1

Table 4. Total LN2 Consumed for Chilldown Process, m_{total}, and percent reduction in LN2 Consumption over the base case, 0L.

P_{in} (psig)		0L	1L	2L	3L	4L
80	m_{total}(kg)	0.75	0.72	0.61	0.56	0.67
	Percent reduction in m_{total}(%)	0	3.5	18.7	25.5	10.8
60	m_{total}(kg)	0.69	0.63	0.53	0.50	0.45
	Percent reduction in m_{total}(%)	0	9.3	23.2	27.4	35.0
40	m_{total}(kg)	0.77	0.54	0.43	0.49	0.40
	Percent reduction in m_{total}(%)	0	29.9	43.6	36.4	47.5
20	m_{total}(kg)	0.74	0.58	0.45	0.40	0.35

Percent reduction in m_{total}(%)	0	20.3	39.0	46.4	53.0

Table 5 lists the total LN_2 consumed and percentage reduction in LN_2 consumption. For the percentage reduction in the cryogen mass used, the minimum is 3.5% for 1L and 80 psig inlet pressure and the maximum is 53% for 4L and 20 psig inlet pressure. Again, it is important to note that for the effects of the coating layers, the percent reduction in cryogen consumption increases with increasing number of coating layers. However, with respect to the coolant mass flow rates, the cryogen consumption reduction increases with decreasing inlet pressure level. As expected these results follow the same trends as those discussed above for the chilldown efficiencies.

The uncertainty for the mass flow rate, γ, was estimated based on the flow meter uncertainty provided by the manufacturer. The relative uncertainties for the mass flow rates are listed in Table 5. The relative uncertainties for the chilldown efficiencies were then estimated and are listed in Table 6. The relative uncertainties for the chilldown efficiencies range between 14.23% and 15.85%.

Table 5. The Relative Uncertainty (%) of the Mass Flow Rate.

P_{in} Psig	0L		1L		2L		3L		4L	
	$\dot{m}$ (kg/s)	γ (%)	$\dot{m}$ (kg/s)	γ (%)	$\dot{m}$ (kg/s)	γ (%)	$\dot{m}$ (kg/s)	γ (%)	$\dot{m}$ (kg/s)	
80	0.0405	3.82	0.0657	2.66	0.0579	2.91	0.0620	2.77	0.0534	3.08
60	0.0356	4.23	0.0484	3.32	0.0485	3.32	0.0531	3.10	0.0502	3.23
40	0.0333	4.47	0.0447	3.53	0.0360	4.19	0.0423	3.68	0.0382	3.99
20	0.0227	6.17	0.0260	5.49	0.0237	5.94	0.0214	6.50	0.0183	7.47

Table 6. The Relative Uncertainty (%) of the Chilldown Efficiency.

P_{in} psig	0L	1L	2L	3L	4L
80	14.49	14.23	14.28	14.25	14.32
60	14.61	14.37	14.37	14.32	14.35
40	14.68	14.42	14.60	14.46	14.54
20	15.28	15.02	15.19	15.42	15.85

4. Conclusion

The experimental results obtained indicate a general trend that the enhancement on heat transfer and improvement on the chilldown efficiency is proportional to the thickness of the low-thermal conductivity coating layer. But there seems to be a tendency that the rate of improvement tapers off as the coating layer gets thicker. An explanation is provided here. Based on the heat transfer physics and a theoretical analysis, there should be an optimal thickness for the low-thermal conductivity coating layer that gives rise to the maximum chilldown efficiency. This optimal thickness would provide the most rapid cooling rate of the bulk tube material. The reason is that there are two heat transfer mechanisms involved that are opposite in nature to each other. The first mechanism is the thermal insulating effect due to the low-thermal conductivity thin layer that facilities a fast drop of the tube inner surface temperature by restricting the heat flow from the bulk of the tube wall to the inner surface. The lower surface temperature allows the quenching process to move from film boiling regime to transition and nucleate boiling regimes. The second mechanism is the conduction of heat from the bulk of the tube wall to the cooling fluid through the inner surface that requires the thermal conductivity of the bulk wall material to be as high as possible such as metals to expedite the wall cooling process. There should exist an optimal thickness of the low-thermal conductivity layer that balances these two competing mechanisms such that the coating is just thick enough to quickly lower the tube surface temperature to that of the Leidenfrost point while it is still relatively thin to not substantially reduce the heat flow from the bulk to the cooling fluid. Another important finding is that the chilldown efficiency and the corresponding reduction in cryogen consumption increase with decreasing inlet pressure and cryogen mass flow rate.

Acknowledgements

This work was partially funded by the NASA MSFC Space Launch System Advanced Development Project under Grant NNM13AA08G with Ms. Melinda Nettles as the Program Director and also by the Andrew H. Hines, Jr./Progress Energy Endowment Fund. Mr. Gary Scheiffelle at the University of Florida Nano Research Facility performed the characterization of coating layer thickness.

References

1. V.P. Carey, *Liquid-Vapor Phase-Change Phenomena*, 2nd ed. New York: Taylor & Francis Group, LLC., 2008.

2. R. Shaeffer, H. Hu, J.N. Chung, An experimental study on liquid nitrogen pipe chilldown and heat transfer with pulse flows, *Int. J. Heat Mass Transf.* 67 (2013) 955–966.

3 S.K. Sahu, P.K. Das, S. Bhattacharyya, An experimental investigation on the quenching of a hot vertical heater by water injection at high flow rate, *Nucl. Eng. Design.* 240 (2010) 1558-1568.

3. C. Agrawal, R. Kumar, A. Gupta, B. Chatterjee, Rewetting and maximum surface heat flux during quenching of hot surface by round water jet impingement, *Int. J. Heat Mass Transf.* 55 (2012) 4772-4782.

4. S.A. Nada, M. Shoukri, A.F. El-Dib, A.S. Huzayyin, Rewetting of hot vertical tubes by a falling liquid film with different directions of venting the geneated steam, *Int. J. Thermal Sci.* 85 (2014) 62-72.

5. K. Yuan, Y. Ji, J. N. Chung, Cryogenic chilldown process under low flow rates, *Int. J. Heat Mass Transf.* 50 (2007) 4011–4022.

6. K. Yuan, Y. Ji, J. N. Chung, Numerical Modeling of Cryogenic Quenching Process in Terrestrial Gravity and microgravity, *International Journal of Heat and Fluid Flow*. 44 (2009) 44-53.

7. H. Hu, J. N. Chung, An experimental study on flow patterns and heat transfer characteristics during cryogenic chilldown in a vertical pipe, *Cryogenics* 52(2012) 268-277.

8. S.R. Darr, H. Hu, N. Glikin, J.W. Hartwig, A.K Majumdar, A.C. Leclair, J. N. Chung, An experimental study on terrestrial cryogenic transfer line chilldown I. Effect of mass flux, equilibrium quality, and inlet subcooling, *Int. J. Heat and Mass Transfer*. 103 (2016) 1225-1242.

9. S.R. Darr, H. Hu, N. Glikin, J.W. Hartwig, A.K Majumdar, A.C. Leclair, J. N. Chung, An experimental study on terrestrial cryogenic transfer line chilldown, II. Effect of flow direction with respect to gravity and new correlation set., *Int. J. Heat and Mass Transfer*. 103 (2016) 1243-1260.

10. S.R. Darr, J. Dong, N. Glikin, J.W. Hartwig, A.K Majumdar, A.C. Leclair, J. N. Chung, The Effect of Reduced Gravity on Cryogenic Nitrogen Boiling and Pipe Chilldown, *Nature Partner Journal (NPJ): Microgravity.* 2 (2016) 16033.

11. S.J. Kim, I.C. Bang, J. Buongiorno, L.W Hu, Effects of nnanoparticle deposition on surface wettability influencing boiling heat transfer in nanofluids, *App. Phys. Lett*. 2006;153107.

12. H.t. Phan, N. Caney, P. Marty, S. Colasson, J, Gavillet, Surface wettability control by nanocoating: The effects on pool boiling heat transfer and nucleation mechanism. *International Journal of Heat and Mass Transfer.* 52 (2009) 5459-5471.

13. J. Bi, K. Vafai, D.M. Christopher, Heat transfer characteristics and CHF prediction in nanofluid boiling, *Int. J. Hear Mass Transfer.* 80 (2015) 256-265.

14. X. Fang, Y. Chen, H. Zhang, W. Chen, A. Dong, R. Wang, Heat transfer and critical heat flux of nanofl uid boiling: A comprehensive review. *Renewable and sustainable Energy Reviews.* 62 (2016) 924-940.

15. X.Q.Wang, A.S. Mujumdar, Heat transfer characteristics of nanofluids: a review. *Int. J. Thermal Science* 46 (2007) 1-19.

16. H. Kim, G. DeWitt, T. McKrell, J. Buongiorno, L.W. Hu, On the quenching of steel and zircaloy spheres in water-based nanofluids with alumina, silica and diamond nanoparticles. *Int. Journal Multiphase Flow* 35 (2009) 427–438.

17. H. Kim, J. Buongiorno, L.W. Hu, T. McKrell, Nanoparticle deposition effects on the minimum heat flux point and quench front speed during quenching in water-based alumina nanofluids. *Int. J. Heat and Mass Transfer.* 53 (2010) 1542–1553.

18. S.Y. Chun, I.C. Bang, Y.J. Choo, C.H. Song, Heat transfer characteristics of Si and SiC nanofluids during a rapid quenching and nanoparticles deposition effects. *Int. J. Heat Mass Transf.* 54 (2011) 1217-1223.

19. R. Chen, M.C. Lu, V. Srinivasan, Z. Wang, H.H. Cho, A. Majumdar, Nanowires for enhanced boiing heat transfer. *Nano Lett.* 9 (2009) 548-533.

20. N.S. Dhillon, J. Buongiorno, F. Varanasi, Critical heat flux maxima during boiling crisis on textre surfaces. *Nat. Commun.* 6 (2015) 8247.

21. S. Mori, Y. Utaka, Critical heat flux enhancement by surface modification in a saturated pool boiling: A review. *Int. J. Heat Mass Transf.* 108 (2017) 2534-2557.

22. H. Hu, C. Xu, Y. Zhao, R. Shaeffer, K.J. Ziegler, J.N. Chung, Modification and enhancement of cryogenic quenching heat transfer by a nanoporous surface. *Int. J. Heat Mass Transf.* 80 (2015) 636–643.
23. H. Hu, C. Xu, Y. Zhao, K.J. Ziegler, J.N. Chung, Boiling and quenching heat transfer advancement by nanoscale surface modification. *Nature, Scientific Reports* 7 (2017) Article Number : 6117.

24. T.L. Bergman, A.S. Lavin, F.P. Incropera, D.P. Dewitt DP, *Fundamentals of Heat and Mass Transfer*. Seventh ed. Weiley (2011).

25. DuPont™ Teflon FEP, Fluoroplastic Film. (2013), WWW.teflon,com/Industrial.